

Efficient electron cyclotron current drive regime for plasma current start-up for fusion reactors

M. Ono^{1, a)}, N. Bertelli¹, V. Shevchenko², H. Idei³, K. Hanada³

¹Princeton Plasma Physics Laboratory, Princeton, NJ, 08543, USA

²Tokamak Energy, UK

³RIAM Kyushu University, Kasuga 816-8580, Japan

^{a)}Corresponding author: mono@pppl.gov

Abstract: Accessibility enhanced efficient fundamental X-mode ECH current start-up regime was identified for reactor-like toroidal magnetic field range which has more than a hundred times higher current drive efficiency compared to more conventional ECH methods for the relevant start-up temperature range. Very high current drive efficiency is possible due to the strong cyclotron interaction only with uni-directional passing electrons constrained by the wave accessibility conditions. This efficient ECCD regime could help facilitate a design of innovative economical solenoid-free tokamak fusion reactor systems.

Introduction: Motivation for non-inductive current start-up and ramp-up is quite well known for tokamaks as the inner high field core region is highly constrained for incorporating adequate central ohmic heating solenoid. The lower-aspect-ratio tokamak is attractive for its high beta stability property which is crucial for economical fusion reactors [1]. In the recent years, a compact cost-effective fusion pilot plant (FPP) is viewed as an important next step for the fusion reactor development path [2]. Recent advances in high temperature superconducting magnet technology allow realization of compact high toroidal field (TF) magnets even for low-aspect-ratio reactor systems. There are several FPP candidate designs already being considered [3-5]. In such studies, a choice of aspect-ratio makes a critical impact on FPP cost performance. If the central solenoid (CS) could be indeed eliminated or significantly reduced, the optimization process of FPP is significantly simplified as the design no longer needs to find the valuable central space for CS and to deal with the serious coil stresses arising from the JxB force interaction of CS-TF coils. For a CS-free tokamak fusion reactor design, it is however necessary to generate ~ 10 MA of toroidal plasma current without CS starting from zero current particularly from low open field electron temperature of ~ 200 eV. There are many possible CS-free tokamak start-up methods which were investigated as summarized in Ref. [1]. Among many start-up options, the electron cyclotron heating (ECH) / electron cyclotron current drive (ECCD) based method might be most reactor compatible from the technology and physics points of view [6-11]. ECH/ECCD-based plasma start-up experiments have been performed at both fundamental and second harmonic EC frequencies [1, 6-11]. Comprehensive reviews of the conventional heating and current drive in the EC range are given [12, 13]. In this letter, we point out a possibility of utilizing extraordinary (X-mode) ECH at fundamental resonance $\omega = \Omega_e$ (X-I) which has an exceptionally high ECH and ECCD efficiency even at the low start-up temperature of sub-keV range for reactor-like high toroidal field systems $\sim 5-6$ T. This mode of heating was proposed previously to create initial start-up plasmas (pre-ionization) to reduce the inductive voltage spike during tokamak start-up phase of ITER [14]. For the X-I accessibility,

due to the $\omega = \Omega_e$ resonance condition, higher field requires high frequency ECCD which has better accessibility to the resonance, and allows the doppler shifted resonance to create efficient current drive

X-I ECH and ECCD for Start-Up: Here we illustrate the effectiveness of X-I ECH and ECCD in Fig. 1 using a typical start-up density of $0.5 \times 10^{13}/\text{cm}^3$ for various representative start-up temperature of $T_{e0} = 200, 500,$ and 800 eVs. Here the wave frequency f is scaled with the toroidal field B_{T0} (i.e., $f = 28 \text{ GHz} \times B_{T0}(\text{T})$) so that the resonance layer position is fixed at $R = 1\text{m}$ with the B_{T0} scan. The launched wave parallel index of refraction is $n_{||0} = 0.4$ which is equivalent to 24° of injection angle. In Fig. 1(a), single path fractional absorption P_{ECH}/P_0 is plotted for X-I and IX-I ECH. For the X-I ECH, the fractional power absorption drastically increases from zero (no absorption) to one (full absorption) as the toroidal magnetic field is increased. The “transition” magnetic field is higher for lower T_{e0} due to the accessibility condition described below. But even at low-end temperature of 200 eV, full absorption can be achieved with $B_{T0} \sim 5\text{-}6$ T toroidal field which is the toroidal magnetic field of ITER and also of typical fusion reactor systems as indicated in the figure. The ST-40 has 3T magnetic field at the magnetic axis but because of being low aspect ratio tokamak, the $5\text{-}6$ T region can still exist within the high-field-side of the plasma. The efficient cyclotron absorption at the low temperature is possible as the X-mode polarization can directly interact with the electron gyro-motion not requiring finite-Larmor-radius (FLR) effects. The corresponding ECH absorption for the second harmonic X-mode (IX-I) using twice the frequency is shown which is an order of magnitude smaller. The IX-I absorption increases with T_{e0} but decreases with the toroidal field B_{T0} due to decreasing plasma dielectric constant. Since IX-I absorption requires the FLR effect, the absorption goes to zero at $T_{e0} = 0$ so the IX-I absorption is relatively low in this lower temperature start-up regime. It should be also noted that the ordinary mode (O-mode) absorption is even lower for both fundamental (I-O) and second harmonics (II-O) and therefore they are not generally being considered for start-up. In Fig 1(b), the corresponding ECCD current (I_{ECCD}) is shown. The X-I I_{ECCD} increases with T_{e0} but remain quite efficient even for low-end temperature of $T_{e0} = 200$ eV at $B_{T0} = 5\text{-}6$ T where the corresponding ECH frequency is about 170 GHz which is the frequency of the ITER ECH system. The corresponding IX-I I_{ECCD} amplified by $\times 100$ is shown in Fig. 1(b). The driven current is indeed very small noting the challenge of IX-I for the sub-keV start-up temperature. In this weakly absorbed regime, IX-I I_{ECCD} is particularly weak due to the generation of relatively balanced opposing ECCD currents at both sides of the resonance which tends to cancel the net driven current. We should also note that the O-mode

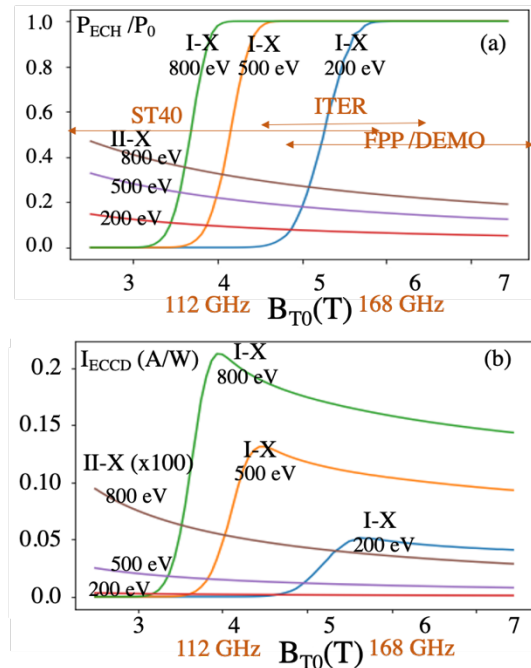


Fig. 1. ECH and ECCD as a function of B_{T0} . $R = 1$ m, $n_{||0} = 0.4$, $n_{e0} = 0.5 \times 10^{19}/\text{m}^3$ and T_{e0} as labeled. (a) Fractional ECH for X-I and IX-I. (b) Corresponding ECCD for X-I and IX-I.

is even lower for both fundamental (I-O) and second harmonics (II-O) and therefore they are not generally being considered for start-up. In Fig 1(b), the corresponding ECCD current (I_{ECCD}) is shown. The X-I I_{ECCD} increases with T_{e0} but remain quite efficient even for low-end temperature of $T_{e0} = 200$ eV at $B_{T0} = 5\text{-}6$ T where the corresponding ECH frequency is about 170 GHz which is the frequency of the ITER ECH system. The corresponding IX-I I_{ECCD} amplified by $\times 100$ is shown in Fig. 1(b). The driven current is indeed very small noting the challenge of IX-I for the sub-keV start-up temperature. In this weakly absorbed regime, IX-I I_{ECCD} is particularly weak due to the generation of relatively balanced opposing ECCD currents at both sides of the resonance which tends to cancel the net driven current. We should also note that the O-mode

ECCD (I-O, II-O) is even smaller than that of IX-I I_{ECCD} . This suggests that it is indeed advantageous to use the X-I start-up as long as the device has a sufficient toroidal magnetic field.

Analysis Tools: In the present analysis, we use the ray-tracing codes which have been shown quite effective in predicting the EC wave propagation, absorption, and current drive. Three ray-tracing codes RT-4 [15], TRAVIS [16], and GENRAY [17] were used in the present work for consistency check and also for the useful utility tools available in these codes. All three ray tracing codes use the cold plasma wave approximation to calculate the wave energy trajectories but use the fully kinetic absorptions in Maxwellian plasmas [18] and utilize the well tested ECCD models [19-23]. A Gaussian profile with edge density and temperature to be 1/10 of that of the central density n_{e0} and temperature T_{e0} was used in our calculations. While all three ray-tracing codes produces essentially the same results, each code has special utilities such as the passing-trapped particle interaction plot provided by the TRAVIS code as shown in Fig. 2. RT-4 uses the initial $n_{||0}$ as the launching condition so it is convenient for the analysis of the wave spectral behavior

while the TRAVIS and GENRAY uses the injection angle as the initial launching condition to tie more directly to the experimental situation. RT-4 was also convenient in scanning of wave and plasma parameters so it was used for Figs. 1, 3 – 4. The injection angle used for TRAVIS and GENRAY is 24° which is equivalent to the launched $n_{||}$ of $n_{||0} = 0.4$ in RT-4. In Fig. 2, we show a case for a Sustained High Power Density (SHPD) tokamak facility [5] with the device major radius of $R_0 = 1.58$ m and $B_{T0} = 5$ T [5]. It should be noted that the current driven tends to scale with $1/R_0$ for other major radius machines. The LFSL fundamental X-mode ray trajectory is shown in Fig. 2(a). For the case of $n_{e0} = 10^{19}/m^3$ and $T_{e0} = 1$ keV, the ray propagates horizontally along the plasma mid-plane and is absorbed, due to the Doppler broadened interactions as described in the accessibility section, completely well before the $n_{||}^2 = R$ cut-off layer as indicated by a red spot in Fig. 2(a). In Fig. 2(b), the radial profile of the absorbed ECH power density is shown. As can be seen in Fig. 2(b), all of the ECH interactions are with the passing particles going in one direction which is favorable for ECCD. The accessibility condition ensured that the absorption occurs always at the low-field-side of $\omega = \Omega_e$ resonance so interacting only with the passing particles moving in one direction. We note that in a tokamak plasma configuration, there are passing and trapped particles where the passing particles undergo spiral orbits along the tokamak flux surface field line and the trapped particles undergo the so-called banana orbits caused by the reflections at the high field region (magnetic “mirror” reflection) along its field line orbit [24]. The passing particles therefore carries most of the plasma currents in tokamaks. If the ECH power is absorbed by the trapped particles, there is no net-current generated so for efficient current drive, it is desirable to heat the passing particles

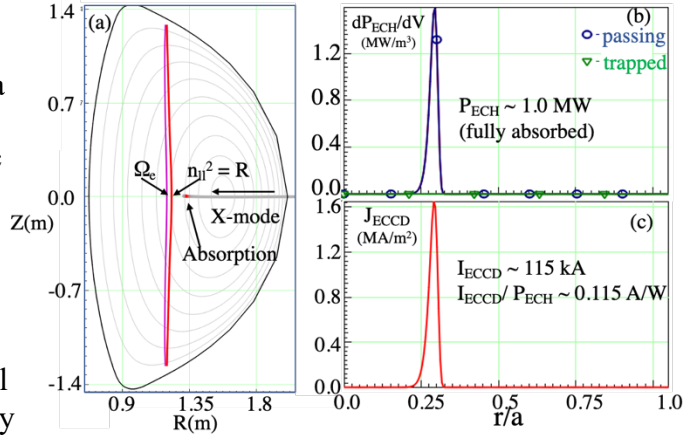


Fig. 2. Propagation, absorption and current drive of X-mode in SHPD with $R = 1.58$ m, $R/a \sim 2$, $B_{T0} = 5$ T, $n_{e0} = 10^{19}/m^3$ and $T_{e0} = 1$ keV, using TRAVIS code. (a) A poloidal cross-section of the LFSL X-mode propagation in a compact pilot plant. The absorption region is indicated in red. (b) Power absorption radial profile. (c) Driven current density profile.

preferentially. This property makes this mode of current drive quite efficient. As shown in Fig. 2(c), the driven current is well localized in front of the resonance and calculated efficiency of 115 kA/MW is quite high for this relatively modest temperature of 1 keV.

$\omega = \Omega_e$ Resonance Accessibility Conditions - Normally, as shown in Fig. 2(a), the low-field-side launched X-mode is reflected at $n_{||}^2 = R \equiv 1 - \omega_{pe}^2 / (\omega(\omega - \Omega_e))$ cut-off layer so that the X-mode does not interact with $\omega = \Omega_e$ resonance [18]. However, if the wave fundamental resonance condition $(\omega - \Omega_e) / (k_{||} V_{e0}) \leq 3$ is satisfied before reaching the $n_{||}^2 = R$ cut-off layer, the fundamental resonant interaction is possible as the wave approaches the reflection point. This resonance condition together with the $n_{||}^2 = R$ cut-off condition yields the following $\omega = \Omega_e$ resonance accessibility condition for plasma density n_{ea} as

$$n_{ea} \leq 37.5 f^2 \frac{V_{e0}}{c} n_{||} (1 - n_{||}^2) \quad (1)$$

The accessibility density is relatively insensitive to $n_{||}$ but depends strongly on f as $\propto f^2$ or B_{T0}^2 where f is the wave frequency in the unit of 100 GHz and n_{ea} is the accessible density in the unit of $10^{19}/m^3$. Since the accessible density goes up with f^2 , the high frequency (or high toroidal field) such as 170 GHz helps to satisfy the accessibility condition even for the relatively low start-up temperatures as shown in Fig. 1. The V_{e0} dependence shows the broadening of the accessibility at higher temperature. It is interesting to point out that this Doppler resonance interaction of LFSL X-mode was observed in WT-3 and TRIAM-1M during ECH application of lower-hybrid wave generated energetic electron plasmas producing efficient ECCD [25,26]. In Fig. 3(a), the ray trajectories for various values of $n_{||0}$ are shown for the SHPD parameters. The ray propagates closer to perpendicular direction for smaller $n_{||0}$ where the ray is purely perpendicular for $n_{||0} = 0$ and purely parallel (toroidal) for $n_{||0} = 1$. As can be seen from Fig. 3(a), the ray propagates closer to the resonance for up to $n_{||0} \leq 0.5$ and the ray is reflected at larger R for higher $n_{||0}$ which suggests decreased interaction for $n_{||0}$ above 0.6 as the ray cannot come sufficiently close to the $\omega = \Omega_e$ resonance. In Fig. 3(b), the absorbed power fraction is plotted as a function of $n_{||0}$ for $n_{e0} = 10^{19}/m^3$ and $T_{e0} = 1$ keV as in Fig. 3. As expected, the power is absorbed fully for $n_{||0} = 0.2 - 0.5$. The resulting ECCD efficiency in MA/MW is plotted in Fig. 3(c) showing efficient ECCD for $n_{||0} = 0.2 - 0.5$. This relative insensitivity with $n_{||0}$ is a very desirable feature indicating that the current drive is not so critically dependent on the launched wave spectrum suggesting one can use a relatively simple waveguide launcher with broader spectra.

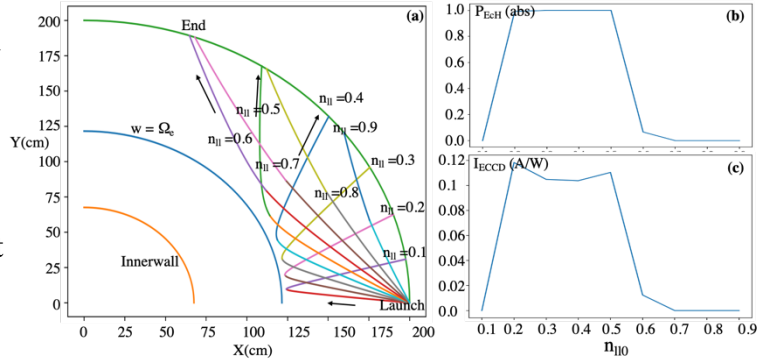


Fig. 3. Propagation, absorption, and current driven for LFSL X-mode as a function of launched $n_{||0}$ as labeled using RT-4 for $n_{e0} = 10^{19}/m^3$ and $T_{e0} = 1$ keV (a) The ray trajectories. (b) Absorbed power. (c) Current driven.

Feasibility of start-up and ramp-up to achieve full SHPD current

–It is now well known that with sufficient ECH power, the

electrons even in the open field line configuration can be heated to about 100 - 200 eV and the subsequent ECH and ECCD can produce a closed flux tokamak configuration as demonstrated in many ECH/EW start-up experiments [6-11]. So, we will start with the low-end temperature of $T_{e0} = 0.1$ and scan up to 1.1 keV. As shown in Fig. 3, the $n_{||0}$ dependence of ECH and ECCD is relatively weak so we assume here that the waves with initial $n_{||0} = 0.4$ (which is equivalent to the launcher angle of 24°). In Fig. 4 (a), we show the ECCD in MW of injected power as a function of plasma density for various start-up electron temperature of $T_{e0} = 0.1$ up to 1.1 keV as marked. The parameter space where the accessibility condition is satisfied is indicated by the solid line which is $n_{e0} \propto T_{e0}^{0.5}$ as shown in Eq. (3). As long as the accessibility condition is satisfied, the ECH absorption is $\sim 100\%$. In the accessible regime, the current driven is roughly proportional to T_{e0} and inversely with density n_{e0} or $I_{ECCD} \propto T_{e0}/n_{e0}$. At the initial low temperature of ~ 100 eV, the accessible density $\sim 0.5 \times 10^{19}/m^3$ but this density is consistent with the initial low-density plasmas in an open field line configuration. Even at such a low temperature range, the I_{ECCD} of ~ 10 kA maybe driven in addition to the pressure driven currents [6, 11]. Once the configuration is closed, then the L-mode scaling [27] can be used to estimate the confinement time of the plasma. It should be noted that the L-mode confinement behaviour is shown to be very robust observed in all kind of auxiliary heated tokamak plasmas as described in Ref [27]. We find that it is always energetically more favorable if the operation can be performed at lower density range as a possible discharge evolution path is marked by an arrow. But as the temperature is increased, this condition can be relaxed as the resonance region expands as shown in Fig. 2.

We shall now try to examine the current ramp-up regime to reach the full current of ~ 10 MA non-inductively. Generated ECCD is plotted in Fig. 4(b) as a function of n_{e0} for $T_{e0} = 1$ keV to

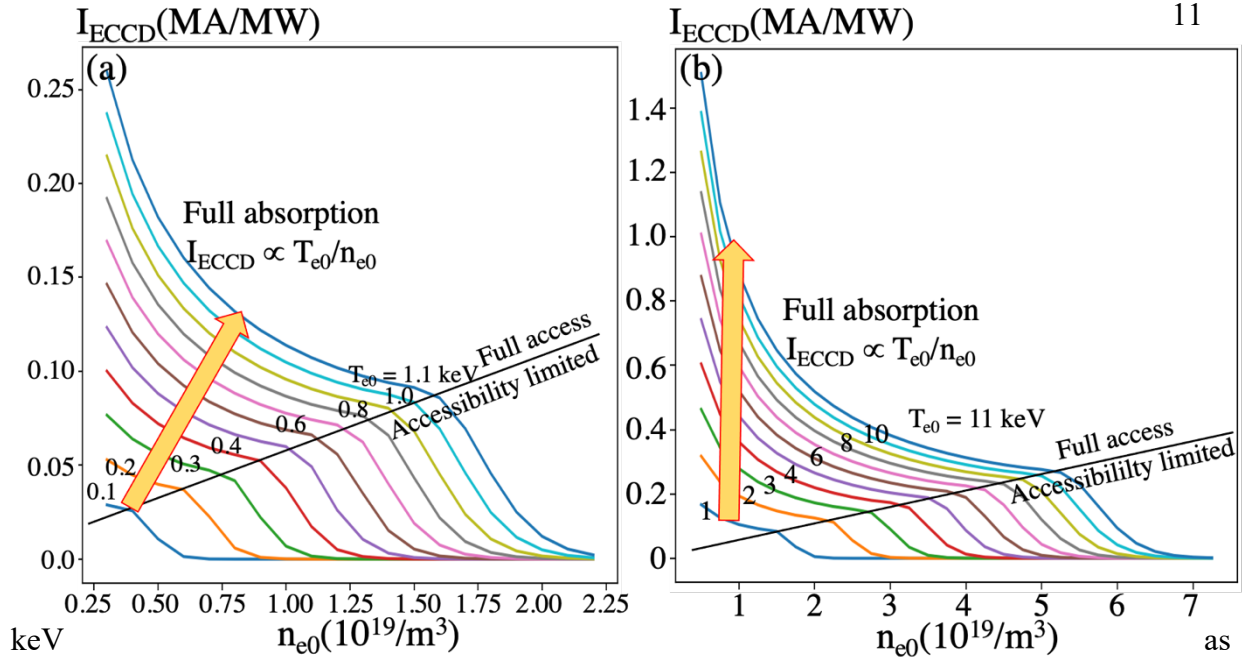


Fig. 4. Temperature and density dependence of X-I I_{ECCD} for $n_{||0} = 0.4$. The accessibility boundary is marked as solid lines. Arrows indicate possible start-up and ramp-up paths. (a) X-I I_{ECCD} for current start-up temperature range of 0.1 - 1.1 keV. (b) X-I I_{ECCD} for current ramp-up temperature range of 1 - 11 keV.

labeled which is within the expected current ramp-up T_{e0} range in SHPD. Once the accessibility limit (as indicated by a line $n_{e0} \propto T_{e0}^{0.5}$) is satisfied, the launched power is fully absorbed, and the driven current follows the usual dependence $I_{ECCD} \propto T_{e0}/n_{e0}$. At lower density the higher MA/MW efficiency can be achieved which is energetically more favorable as indicated by an arrow as a possible discharge evolution path. The suggested ECCD start-up and current ramp-up paths shown in Fig. 4 is energetically accessible as the required heating power for L-mode-type confinement is considerably smaller than the applied power of 10 MW. It is therefore indeed possible to generate ~ 10 MA of ECCD with 10 MW of applied power at $n_{e0} \sim 1 \times 10^{19}/m^3$ for $T_{e0} \sim 10$ keV. In the present analysis, the bootstrap and pressure driven currents are not included but they could provide additional currents further relaxing the required I_{ECCD} [6].

Quasi-linear evolution and ECCD enhancement

– The analysis thus far uses the Maxwellian velocity distribution for ECH and ECCD. The ECH could generate tail electrons which could further expand into higher velocity space which to enhance ECCD. We investigated the quasi-linear diffusion ECCD enhancement using the CQL3D code [28]. In Fig. 5(a) the resulting velocity distribution is shown for $n_{e0} = 1 \times 10^{19}/m^3$ at $T_{e0} = 1$ keV and $P_{INJ} = 1$ MW with 24° injection angle (which is equivalent to $n_{||0} = 0.4$) and an ensemble of 20 rays. As can be seen from the figure, the accelerated electrons are all in the passing particles and only in one direction in the velocity space. This results in very high current drive efficiency as shown in Fig. 5(b) where the driven current is 450 kA which is about x4 increase from the comparable Maxwellian linear value of ~ 110 kA shown in Fig. 2(c) or 4(d). The current profile is relatively localized but somewhat broader than the linear absorption profile shown in Fig. 2(c). In Fig. 5(c), enhancements due to the CQL3D calculations compared to the linear calculations

are shown for various T_{e0} as labeled. The CQL3D indeed enhances the current drive in a whole temperature range though it tends to give more fractional increase at lower T_{e0} range which would be particularly favorable for the start-up regime. Together with further expected enhancements with bootstrap currents, it appears therefore to be feasible to generate ~ 10 MA fully non-inductively with relatively modest power of ~ 10 -20 MW for a solenoid-free compact SHPD.

Conclusions and Discussions – The elimination of OH solenoid maybe the most impactful design driver for the realization of economical compact fusion tokamak reactor systems. However, this would require plasma start-up and current ramp-up from zero plasma current and low electron temperature of sub-keV to the full plasma current ~ 10 MA completely non-inductively. To address this challenge, an efficient solenoid-free start-up and ramp-up scenario

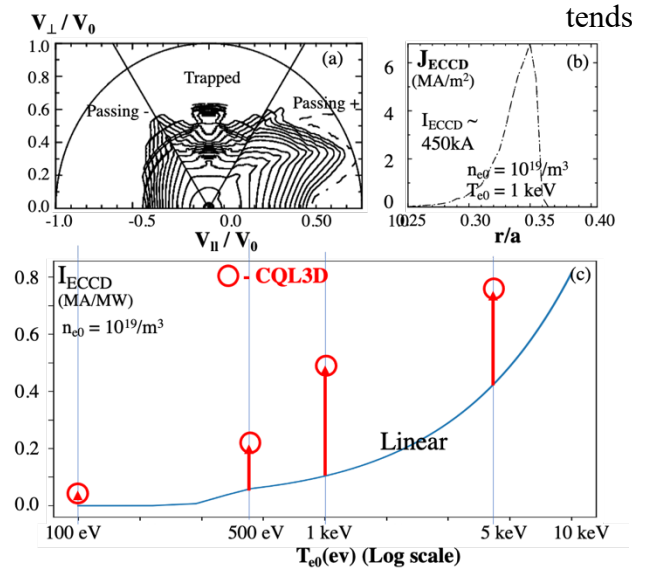


Fig. 5. CQL3D calculations for $n_{e0} \sim 10^{19}/m^3$. (a) Velocity distribution $T_{e0} \sim 1$ keV. (b) Corresponding current drive density. (c) Current driven as a function of temperature as labeled. The line is linear and red circles are CQL3D values.

utilizing the LFSL X-I-mode is proposed to generate ~ 10 MA of plasma current for a compact SHPD with relatively modest ECH power of $\sim 10 - 20$ MW utilizing the presently available 170 GHz gyrotrons developed for ITER. The present concept of X-I ECCD is more than two orders of magnitude higher in efficiency compared to other more conventional ECCD such as I-O or IX-I in the plasma start-up parameters in the reactor-grade toroidal field regimes. The ECH approach is generally favorable from the well understood wave coupling, propagation, and absorption physics. The wave accessibility density limit improves significantly at higher B_{T0} as accessible density goes up as f^2 (or as B_{T0}^2) that enables the current start-up and ramp-up to operate in a reasonable plasma density of $\sim 0.5 - 1.0 \times 10^{19}/m^3$ with a very high ECH/ECCD efficiency at 170 GHz for $B_{T0} \sim 5-6$ T. The high ECCD efficiency is due to the strong wave-particle interactions at the Doppler broadened $\omega = \Omega_e$ resonance, due to the strong cyclotron interaction, together with absorption on uni-directional passing electrons which results from the wave accessibility constraint. The ECCD efficiency of X-I is more than 100 times better than more conventional ECH/ECCD such as O-I, X-II, O-II in this sub-keV start-up regime. The quasi-linear analysis using CQL3D shows further enhancements of ECCD efficiency over the linear calculations due to the generation of less collisional higher energy tail electrons. The current drive efficiency remains high for a broad range of $n_{||0}$ (or injection angle) suggesting that a relatively simple waveguide launcher could be used. Together with the relatively simple waveguide coupling physics in ECH-based system which would greatly facilitate the optimization of the economical compact fusion reactor design. Since the LFSL X-I ECCD region is well localized near the $\omega = \Omega_e$ resonance region, it is also possible to control the current drive profile if desirable by aiming the waveguide launchers on/off machine midplane. This may also lead to more favorable current profiles needed for the advanced tokamak operation. With the advent of higher field ST facilities such as ST-40 [29], the present concept could be tested in the near future. Once the ramp-up to the full plasma current is achieved, the same ECH system can be switched to more conventional ECH and ECCD such as the O-mode which would permit the access to high density $\sim 2-3 \times 10^{20}/m^3$ or more advanced EBW-based scenarios [11] for even higher density steady-state operations [30]. The present X-I could also be applied to ITER as generating start-up current ECCD would potentially help optimize the plasma operations. As noted above, the X-I ECCD could be switched to the I-O ECCD [16] for the main plasma operations using polarizers.

ACKNOWLEDGMENTS

This work supported by DoE Contract No. DE-AC02-09CH11466. The authors thank the ST-40 ECH and ECCD discussions with Drs. S. Shiraiwa, J. Menard, S. Kaye, B. Grierson, S. Diem, S. McNamara, and P. Thomas. One of the authors (N.B.) thanks Dr. N. B. Marushchenko for providing the TRAVIS source code.

REFERENCES

- [1] M. Ono and R. Kaita, *Physics of Plasmas* **22**, 040501 (2015).
- [2] see for example, https://usfusionandplasmas.org/FESAC_Report_2020_Powering_the_Future.pdf, and <https://www.nap.edu/read/25991/chapter/1>
- [3] J.E. Menard, et al, *Nucl. Fusion*, **56** 106023 (2016).
- [4] R.J. Buttery, et al, *Nucl. Fusion*, **61** 046028 (2021).

- [5] J.E. Menard, et al, *IAEA-CN-286/1013*, IAEA (2021).
- [6] C. B. Forest , et al., *Physics of Plasmas* **1**, 1568 (1994)
- [7] T. Yoshinaga, et al., *Phys. Rev. Lett.* **96**, 125005 (2006).
- [8] H. Idei et al.,*Nucl. Fusion* **57** 126045 (2017).
- [9] M. Ishiguro, et al., *Physics of Plasmas* **19**, 062508 (2012).
- [10] T. Bigelow, et al., *Bull. Am. Phys. Soc.* **58**, BP8.00076 (2013).
- [11] V.F. Shevchenko, et al., *Nucl. Fusion* **50** 022004 (2010).
- [12] R. Prater, *Physics of Plasmas* **11**, 2349 (2004)
- [13] M. Bornatici et al, *Nucl. Fusion* **23** 1153 (1983).
- [14] T. Maekawa, et al., *Nucl. Fusion* **58** 016037 (2018).
- [15] M. Ono, et al., *AIP Conference Proceedings* **2254**, 090001 (2020).
- [16] N. B. Marushchenko et al, *Comp. Phys. Comm.* **185**, 165 (2014).
- [17] A. P. Smirnov and R. W. Harvey, *Bull. Am. Phys. Soc.* **40**, 1837 (1995).
- [18] T.H. Stix, *Waves in Plasmas* (American Institute of Physics, New York, 1992).
- [19] N.J. Fisch and A.H. Boozer, *Phys. Rev. Lett.* **45** 720 (1980).
- [20] R. Prater et al, *Nucl. Fusion* **48** 035006 (2008).
- [21] R.H. Cohen, *Phys. Fluids* **30** 2442 (1987).
- [22] Y.R. Lin-Liu, V.S. Chan, and R. Prater, *Phys. Plasmas***10** 4064 (2003).
- [23] N. B. Marushchenko et al, *Physics of Plasmas* **18**, 032501 (2011).
- [24] J. Wesson, *Tokamaks*, Oxford University Press, Fourth Edition (2011).
- [25] T. Maekawa, et al., *Phys. Rev. Lett.* **70**, 2561 (1993).
- [26] H. Idei, K. Hanada et al.,*Nucl. Fusion* **46** 489 (2006).
- [27] S. M. Kaye et al., *Nucl. Fusion* **37** 1303 (1997).
- [28] Y. V. Petrov and R. W. Harvey, *Plasma Phys. Control. Fusion* **58** 115001 (2016).
- [29] M. Gryaznevich, et al., *Fusion Engineering and Design* **123** 177 (2017).
- [30] V.F. Shevchenko et al., *Phys. Rev. Lett.* **89**, 265005 (2002).